Influence of the bonding front propagation on the wafer stack curvature

E. Navarro, Y. Bréchet, A. Barthelemy, I. Radu, T. Pardoen, and J.-P. Raskin

Citation: Applied Physics Letters **105**, 061908 (2014); doi: 10.1063/1.4893462
View online: http://dx.doi.org/10.1063/1.4893462
View Table of Contents: http://scitation.aip.org/content/aip/journal/apl/105/6?ver=pdfcov
Published by the AIP Publishing

Influence of the bonding front propagation on the wafer stack curvature

E. Navarro,[1,2] Y. Bréchet,[2] A. Barthelemy,[1] I. Radu,[1] T. Pardoen,[3] and J.-P. Raskin[4]
[1]*SOITEC—Parc Technologique des Fontaines, 38190 Bernin, France*
[2]*SIMaP—Grenoble-INP, 1340 rue de la Piscine, 38402 St. Martin d'Hères, France*
[3]*Institute of Mechanics, Materials and Civil Engineering (iMMC), Université catholique de Louvain, B-1348 Louvain-la-Neuve, Belgium*
[4]*Institute of Information and Communication Technologies, Electronics and Applied Mathematics (ICTEAM), Université catholique de Louvain, B-1348 Louvain-la-Neuve, Belgium*

(Received 23 May 2014; accepted 7 August 2014; published online 14 August 2014)

The influence of the dynamics of the direct wafer bonding process on the curvature of the final wafer stack is investigated. An analytical model for the final curvature of the bonded wafers is developed, as a function of the different load components acting during the bonding front propagation, using thin plate theory and considering a strain discontinuity locked at the bonding interface. Experimental profiles are measured for different bonding conditions and wafer thicknesses. A very good agreement with the model prediction is obtained and the influence of the thin air layer trapped in-between the two wafers is demonstrated. The proposed model contributes to further improvement of the bonding process, in particular, for the stacking of layers of electronic devices, which requires a high accuracy of wafer-to-wafer alignment and a very low distortion level. © *2014 AIP Publishing LLC*. [http://dx.doi.org/10.1063/1.4893462]

Direct bonding is commonly used to assemble semiconductor wafers, such as in the fabrication of silicon-on-insulator wafers (SOI). It constitutes a promising solution to stack several integrated circuit layers, in order to build high density three dimensional integrated device (3D-IC).[1,2] To be successful, the bonding process requires accurate alignment and very low mechanical distortion. Therefore, a complete understanding and quantitative modelling of the mechanics involved during the direct bonding process is essential.[3,4]

It has been previously observed that the bonding process could induce a residual deformation of the final bonded wafers pair. A first mechanical model has been proposed by Turner *et al.*, considering the curvature induced by the chucking system.[5,6] Nonetheless, the influence of the dynamics behavior of the direct wafer bonding process, in particular, the bonding front propagation, has not yet been addressed.

When the two wafers are brought into contact, a thin air layer remains trapped in between them, preventing immediate contact. Hence, an external force must be applied locally to initiate a first contact point. Then, adhesion forces drive the expansion of the contacted area to the entire wafer area, leading to the bonding front propagation or "contact wave."[7,8] During the propagation, both wafers are significantly deformed in the vicinity of the bonding front, by both the adhesion forces and the pressure coming from the thin film of fluid.[8]

In this paper, a model is proposed to take into account the bonding front propagation effect on the final wafer stack curvature. In addition, the model is validated by accurate experimental measurements. The results are presented and discussed in the following.

The main idea of the model is to consider that the two wafers are progressively joined together, while the macroscopic curvatures can be different. Therefore, a strain discontinuity can be locked at the bonding interface, depending on the different loads acting on the wafers during the bonding propagation. The expected wafer shape at the vicinity of the bonding front is illustrated in Fig. 1.

The thin plate theory provides an accurate description of the wafer mechanics at the macroscopic scale. Both wafers are curved by the moments acting near the bonding front, M_1 and M_2, including the action of gravity, the fluid pressure and the support reactions. Therefore, the deformation of the inner surface of each wafer i can be evaluated using the relationship $\epsilon_i = \pm k_i t_i/2$, where t_i is the wafer thickness and $k_i = M_i/D_i$ is the curvature of the wafer with $D_i = E_i t_i^3/12(1-\nu_i^2)$ is the flexural rigidity of the wafer i (E_i and ν_i are the Young's modulus and Poisson ratio). The sign is positive for the top wafer and negative for the bottom wafer.

Nonetheless, the plate theory is not sufficient to explain how this deformation is transferred and locked by the bonding interface. Indeed, two ideal quadratic surfaces have one contact point only. Since the wafers are elastically deformable, and because adhesion forces tend to pull the two surfaces into contact, there is a finite contact area between the

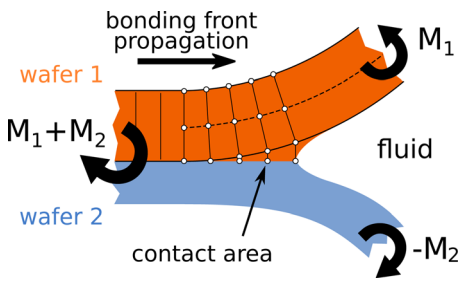

FIG. 1. Schematic representation of the cross-section near the bonding front. The solid line represents the shape predicted by thin plate theory, while the filled area is the expected real shape. The scale of this picture is exaggerated on purpose. The expected wafer thickness variation is more than one thousand times smaller than the wafer thickness. The sign convention for the moments is that a positive moment induces a positive curvature (i.e., a "U" shape).

two curved wafers. This idea has analogy with the Derjaguin, Muller, and Toporov model (DMT) or the Johnson, Kendall, and Roberts model (JKR) which are both used to study the adhesive contact of an elastic spherical particle to a plane surface.[9,10]

As a result, the contact between the two wafers occurs while they are both bent with two different macroscopic curvatures. Because the vertical displacement due to the adhesion forces is small in comparison to the plate deformation, the in-plane strain is expected to be partly maintained when the bonding interface is created, and a strain discontinuity, noted $\Delta\epsilon$, is then locked at the bonding interface while the bonding front propagates over the entire wafer area.

If absolutely no sliding at the interface, nor shear relaxation, occurs after the formation of the bonded interface, the strain discontinuity writes

$$\Delta\epsilon_{no\ slidding} = \epsilon_1 - \epsilon_2 = \frac{t_1}{2}\frac{M_1}{D_1} + \frac{t_2}{2}\frac{M_2}{D_2}. \quad (1)$$

In the case of relaxation or sliding occurring at the bonding interface, the bilayer can be seen as a single plate with equivalent stiffness $D_1 + D_2$. In this case, both wafers have the same curvature when the interface is being locked, $(M_1 + M_2)/(D_1 + D_2)$, and the strain discontinuity writes

$$\Delta\epsilon_{sliding} = \frac{t_1 + t_2}{2}\frac{M_1 + M_2}{D_1 + D_2}. \quad (2)$$

The two situations described above (with or without interface sliding) represent the two extreme cases of the model.[11] The actual behavior of the bonding front at the nanoscale is not known. Therefore, a phenomenological coefficient ϕ is introduced to describe the expected real strain discontinuity (with $\phi \in [0, 1]$):

$$\Delta\epsilon(\phi) = \phi\,\Delta\epsilon_{sliding} + (1 - \phi)\,\Delta\epsilon_{no\ sliding}. \quad (3)$$

The next part of the model derivation consists of connecting the strain discontinuity $\Delta\epsilon$ to the internal moment M_i which is responsible for the final curvature of the stack. This derivation is analogous, for instance, to the problem of thermal stress in a multilayer plate.[12] Here, a simple relationship is obtained in terms of the flexural rigidities only, by considering that the two-plate elements are joined together while they are both deformed at the same virtual curvature $k^\star$. The strain discontinuity at the interface writes, in this case $\Delta\epsilon = k^\star(t_1 + t_2)/2$. By writing the linear plate equations at the instant of bonding $M_1^\star = D_1\,k^\star$, $M_2^\star = D_2\,k^\star$ and $M_1^\star + M_2^\star + M_i = D_{12}k^\star$ where D_{12} is the flexural rigidity of the assembled stack,[13] the following relationship is obtained[11]:

$$M_i = 2\,\frac{D_{12} - D_1 - D_2}{t_1 + t_2}\,\Delta\epsilon. \quad (4)$$

The final part of the derivation is to apply the thin plate equation to the specific experimental situation. Because all external forces acting on the wafers during the bonding have to be known, we have used a bonding configuration with a single central pointwise support for the bottom wafer. Then, the support reaction force is always the same whatever the shape taken by the wafers and has no influence on the bonding dynamics. An illustration of the corresponding bonding sequence is shown in Fig. 2.

Moreover, in this configuration, there is no need to apply an external force to initiate the bonding. This can be understood by considering that the weight of the top wafer is transferred to the bottom wafer by the fluid pressure. Then, the bending of the bottom wafer is more pronounced than the top one. The air layer thickness profile takes a trumpet shape, dictating the direction of the air flow. With 200 mm diameter wafers, spontaneous initiation is observed less than 30 s after the wafer release.

The moment induced by the fluid M_{fluid} could seem difficult to estimate. However, a simple relationship between the work of adhesion W and the moment acting on the adhesion boundary has been previously derived using an energy balance[14] and by considering that the remaining strain energy per unit area in the bonded plates and the strain energy per unit area due to the gravity are negligible compared to the magnitude of the work of adhesion

$$M_{fluid} = \sqrt{2W\frac{D_1 D_2}{D_1 + D_2}}. \quad (5)$$

Therefore, the effect of the fluid is assumed to be constant over the position along a radius of the wafer, while the moments due to gravity, $M_{g1}(r)$ and $M_{g2}(r)$, are function of the bonding front position r. Then, the loads acting on the bonding front write

$$\begin{aligned} M_1(r) &= +M_{fluid} + M_{g1}(r), \\ M_2(r) &= -M_{fluid} + M_{g2}(r). \end{aligned} \quad (6)$$

The thin plate equations for cylindrical symmetry[13] are solved, separately, in the case of a uniform pressure $p^\star$ and in the case of a uniform moment $m^\star$

$$\Delta\Delta w_g = p^\star/D_{12}, \quad (7)$$

$$\frac{\partial^2 w_{fluid}}{\partial r^2} + \frac{\nu}{r}\frac{\partial w_{fluid}}{\partial r} = -m^\star/D_{12}, \quad (8)$$

where Δ is the Laplacian operator, $w(r)$ is the wafer deflection, and ν is the Poisson ratio. The corresponding gravity and fluid contributions are obtained as

$$w_g(r) = -\frac{p^\star r^2 R^2}{64\,D_{12}}\left[\left(\frac{r}{R}\right)^2 + 2\frac{3+\nu}{1+\nu} - 8\,ln\left(\frac{r}{R}\right)\right], \quad (9)$$

$$w_{fluid}(r) = -\frac{m^\star r^2}{2(1+\nu)\,D_{12}}, \quad (10)$$

where R is the radius of the wafer.

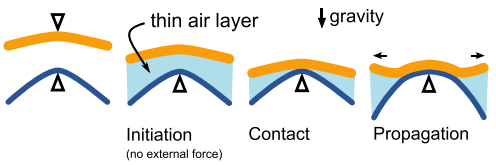

FIG. 2. The bonding sequence with a single central pointwise support configuration. The triangle represents the support. Both wafers are initially flat and the downward curvatures are induced by gravity only.

The expressions for the moment $m^\star$ and for the uniform load $p^\star$ are deduced from the internal moment (Eq. (4)) and by using the linear property of the plate equation

$$m^\star = A\,(1-\phi)\left(\frac{t_1}{D_1}-\frac{t_2}{D_2}\right)M_{fluid}, \tag{11}$$

$$p^\star = A\left[\phi\frac{(t_1+t_2)^2}{D_1+D_2}+(1-\phi)\left(\frac{t_1^2}{D_1}+\frac{t_2^2}{D_2}\right)\right]\rho g, \tag{12}$$

where ρ is the material density, g is the gravity constant, and $A=(D_{12}-D_1-D_2)/(t_1+t_2)$. Finally, the total wafer deflection is obtained by summing the fluid and gravity contributions.

It should be noted that in the case of similar wafers (i.e., same thickness and same flexural rigidity) the effects of the propagation (M_{fluid}) and of the sliding coefficient ϕ disappear from the equations (see Eqs. (11) and (12)). For this reason, wafers with different thicknesses are used for the experiments. Bulk silicon wafers, 500 μm and 717 μm thick, 200 mm in diameters are used. The crystal orientation of the surface plane is (100). A standard cleaning (RCA) is performed before bonding. The work of adhesion is measured equal to $W\approx 90\,\text{mJ/m}^2$. The measured wafer thickness variation is less than ± 1 μm, and the measured bow, prior to bonding, is less than 5 μm for both wafer thicknesses.

The central support is a simple polymer element with about 2 mm height and 5 mm diameter. No contact is observed between the bottom wafer and the bottom support plate.

A mechanical profilometer (KLA-Tencor P16) is used to measure the final shape of the bonded wafers. In order to correct for the effect of gravity during the measurement, the wafers lay on a three-point support, and the measurements are made on both sides of the wafer stack. The average of the two profiles gives the wafer shape without any effect of gravity.

Four bonding permutations are possible, relative to gravity, with two different wafer thicknesses: 717/717 μm, 717/500 μm, 500/717 μm, and 500/500 μm.

Fig. 3 shows the results for the wafer profile measurements along the $\langle 110\rangle$ crystal direction. All four bonded wafer pairs exhibit a different profile, ranging from about -100 μm to $+20$ μm bow (from center to edge). The 500/717 μm bonding has the most complex shape. The curvature is positive except near the wafer center where it is negative. This is the only permutation where the resulting bow is positive. Both the 717/717 μm and the 500/500 μm configurations have a similar shape, with different amplitudes. Wafers are curved downward, and the curvature becomes almost zero at the outer periphery of the wafers. The configuration 717/500 μm is the most curved bonded pair, with a bow of about -100 μm. The shape is almost a pure quadratic curve (constant curvature).

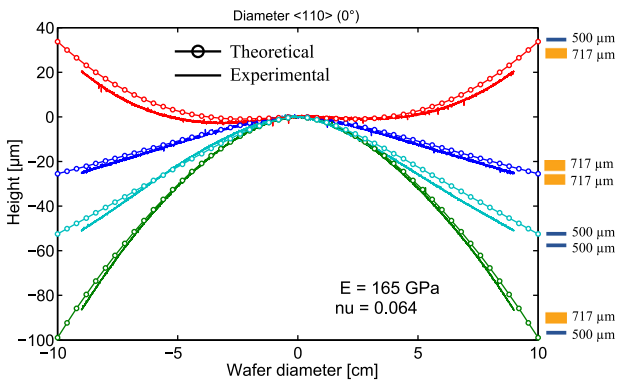

FIG. 3. Results for the four thickness permutations relative to gravity. Measurements are made perpendicular to the notch direction, i.e., in the $\langle 110\rangle$ crystal direction, with a correction for the effect of gravity. Circles indicate the theoretical prediction using $W=90\,\text{mJ/m}^2$ and $\phi=0.67$.

In the case of dissimilar wafer thicknesses, the bonded stack is curved towards the thin wafer. The thinner wafer is more curved during the bonding (because of the smaller flexural rigidity), and thus, its inner surface is more stretched when it is brought in contact with the other wafer. The model provides a very good description of the experimental results.

The model quantitatively reproduces the experiments when using the work of adhesion value $W=90\,\text{mJ/m}^2$ and an adjusted sliding coefficient $\phi=0.67$, see Fig. 3. The silicon Young's modulus along the $\langle 110\rangle$ direction is taken equal to $E_{110}=165$ GPa and the Poisson ratio is equal to $\nu_{110}=0.064$.[15]

The sliding coefficient value $\phi=0.67$ means that the actual behaviour of the bonding front is in between the two extreme cases considered in the derivation of the model. For example, for the 717/500 μm bonding configuration, the bow will vary from -32 μm in the case of a pure sliding interface (i.e., $\phi=1$), to -197 μm in case of a no sliding interface, while the measured bow is about -100 μm. Additional studies are needed to build a sound physical meaning of the sliding coefficient ϕ and its dependencies on the parameters of the problem.

In order to demonstrate the unique effect of the bonding propagation on the final curvature of the stack, a bonding test was performed along a vertical plane. Hence, the effect of gravity is eliminated. Two silicon wafers are first bonded using the conventional horizontal bonding method. Afterwards, the bonded pair is placed vertically and manually held from the upper side. The wafers are partially separated (one or two centimeters from the edge) by inserting a polymer blade from the bottom edge. After separation, the blade is removed and the wafers re-bonded, while still being maintained at the upper edge. Experiments have been performed in the case of similar wafers (717/717 μm) and in the case of dissimilar wafers (500/717 μm). The obtained profiles are presented in Fig. 4.

In the case of similar wafers, the resulting final bonded shape deflection is about ± 2 μm, which is of the same order of magnitude as the pre-bond bulk wafer flatness and thickness variation, and within the measurement error. As expected, a symmetric bonding configuration leads to a flat final bonded wafer shape.

In the case of dissimilar wafers, the situation is not symmetric anymore. As predicted by the model, the final stack is curved towards the side of the thin wafer and most significantly curved along the propagation direction than along the transverse direction. However, because the axisymmetric assumption is not valid anymore for the vertical configuration, only an estimate of the final wafer profile can be obtained using the present model.

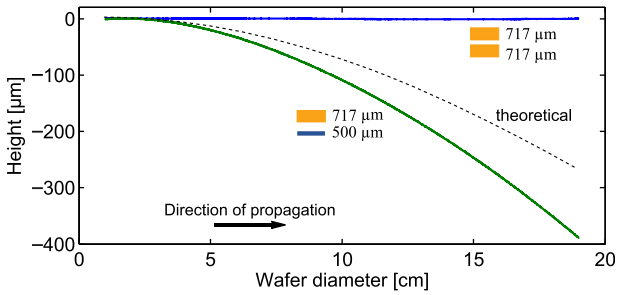

FIG. 4. Wafer profiles corresponding to the vertical bonding configuration. Experimental results are measured on the diameter along the direction of propagation (solid line). The dashed line indicates a theoretical estimate for the dissimilar wafers case obtained using the same parameters as before.

As a conclusion, an analytical model is proposed to explain the residual curvature of bonded wafers for the specific case of direct wafer bonding. Due to the bonding front propagation, both wafers are significantly curved in the vicinity of the bonding front and, consequently, a strain discontinuity can be progressively locked at the interface. Because of the elastic deformation of the wafer around the bonding front, the in-plane deformation due to the bending of the wafer is transferred to the bonding interface. As a consequence, the propagation can have a significant effect on the final curvature of the stack, in particular, when the two wafers are dissimilar or if one is clamped to a support. A specific bonding configuration has been used, in such a way that all the loads acting on the wafers during the bonding are known. Two different thicknesses have been considered for the silicon wafers and pairs of wafers have been bonded with four different permutations. A very good agreement between theory and experiments is obtained for the four bonding permutations.

Additional work should address the relaxation by sliding of the bonding interface and improve the mechanical description of the bonding front at the micrometer scale. Additional experiments are possible to extend and validate the model to other situations, as, for example, to modify the work of adhesion, the wafer material properties and the wafer support configuration. The final objective is to design bonding configurations that limit the final curvature of the assembled stack and allow for enhanced alignment accuracy.

[1]S. J. Koester, A. M. Young, R. R. Yu, S. Purushothaman, K.-N. Chen, D. C. J. La Tulipe, N. Rana, L. Shi, M. Wordeman, and E. J. Sprogis, IBM J. Res. Dev. **52**, 583 (2008).
[2]C. S. Tan, R. J. Gutmann, and L. R. Reif, *Wafer Level 3-D ICs Process Technology* (Springer, 2008).
[3]M. Broekaart, A. Castex, K. Landry, R. Fontaniere, and C. Lagahe-Blanchard, ECS Trans. **50**, 371 (2013).
[4]G. Gaudin, G. Riou, D. Landru, C. Tempesta, I. Radu, M. Sadaka, K. Winstel, E. Kinser, and R. Hannon, in *2010 IEEE International 3D Systems Integration Conference (3DIC)* (2010), pp. 1–4.
[5]K. T. Turner and S. M. Spearing, J. Appl. Phys. **92**, 7658 (2002).
[6]K. T. Turner, M. D. Thouless, and S. M. Spearing, J. Appl. Phys. **95**, 349 (2004).
[7]F. Rieutord, B. Bataillou, and H. Moriceau, Phys. Rev. Lett. **94**, 236101 (2005).
[8]E. Navarro, Y. Bréchet, R. Moreau, T. Pardoen, J.-P. Raskin, A. Barthelemy, and I. Radu, Appl. Phys. Lett. **103**, 034104 (2013).
[9]B. Derjaguin, V. Muller, and Y. Toporov, J. Colloid Interface Sci. **53**, 314 (1975).
[10]K. L. Johnson, K. Kendall, and A. D. Roberts, Proc. R. Society of London, Ser. A **324**, 301 (1971).
[11]See supplementary material at http://dx.doi.org/10.1063/1.4893462 for additional illustrations.
[12]L. B. Freund and S. Suresh, *Thin Film Materials: Stress, Defect Formation and Surface Evolution* (Cambridge University Press, 2003), p. 87.
[13]E. Ventsel and and T. Krauthammer, *Thin Plates and Shells: Theory, Analysis, and Applications* (2001), p. 684.
[14]C. Majidi and G. Adams, Mech. Res. Commun. **37**, 214 (2010).
[15]M. A. Hopcroft, W. D. Nix, and T. W. Kenny, J. Microelectromech. Syst. **19**, 229 (2010).